ARTICLE

Intercalative Poly(carbazole) Precursor Electropolymerization within Hybrid Nanostructured Titanium Oxide Ultrathin Films

Antonio F. Frau, Nicel C. Estillore, Timothy M. Fulghum, and Rigoberto C. Advincula*

Department of Chemistry and Department of Chemical and Biomolecular Engineering, University of Houston, Houston, Texas 77204-5003, United States

ABSTRACT A protocol for nanostructuring and electropolymerization of a hybrid semiconductor polycarbazole-titanium oxide ultrathin film is described. Ultrathin (<100 nm) films based on polycarbazole precursor polyelectrolytes and titanium oxide (TiO_x) have been fabricated by combining the layer-by-layer (LbL) and surface sol−gel layering techniques. Film growth was followed and confirmed through UV−vis spectroscopy, ellipsometry and quartz crystal microbalance with dissipation (QCM-*D*). Subsequent anodic electrochemical oxidation of the carbazole pendant units afforded a conjugated polymer network (CPN) film within intercalating TiO_x layers of cross-linked and π-conjugated carbazole units. Cyclic voltammetry (CV), UV−vis, and fluorescence spectroscopy measurements confirmed this process. The LbL-driven polyelectrolyte deposition process resulted in a quantified electrochemical response, proportional to the number of layers, while the TiO_x acted as a dielectric spacer limiting electron transfer kinetics and attenuating energy transfer in fluorescence. Electro-optical properties were compared with other polycarbazole thin film materials with respect to bandgap energy (E_g). The straightforward protocol in film nanostructuring and barrier/dielectric properties of the inorganic oxide slab (denoted here as, TiO_x) should enable applications in organic light-emitting diodes (OLEDs), dielectric mirrors, planar waveguides, and photovoltaic devices for these hybrid ultrathin films.

KEYWORDS: hybrid • nanostructure • electropolymerization • polycarbazole • QCM • intercalation

INTRODUCTION

Novel or smart materials based on nanostructured or layered components are of high importance toward miniaturization (1−5) and nanomanufacturing. The assembly of hybrid, organic−inorganic, and nanostructured films can be a challenge (6−9). Such assembly may require macromolecular and molecular synthetic techniques from two different media or dispersions (10). Nevertheless, combining two dissimilar materials may result in unusual physical properties or nanoscale phenomena (11). By comparing the efficiency of ultrathin and multilayered films to their bulk counterparts, it is possible to identify new structure−property relationships for applications in chemical sensors (12), microelectronics (13, 14), and nonlinear optics (15) to name a few. The layer-by-layer (LbL) film deposition is a most versatile and facile process for building up films of polymers or inorganic materials (1−5, 16, 17). Unlike the Langmuir−Blodgett (LB) technique, which necessitates an air−water interface (18, 19), the LbL assembly of charged species as alternating layers can yield highly complex, layered architectures via simple dipping procedures from aqueous solutions, resulting in structures held together primarily by electrostatic forces (1−5). Further film stability can be ensured by stronger interactions such as ionic bonds, charge-transfer, and hydrogen/coordination bonds (20−23). A wide variety of spectroscopic and surface-sensitive/microscopic techniques have been utilized for investigating and characterizing these systems, along with quartz crystal microbalance (QCM) (24, 25), ellipsometry (26), surface plasmon resonance (SPR) spectroscopy (27), and atomic force microscopy (AFM) imaging.

One of the unique features of organic−inorganic hybrid materials is the possibility of fine-tuning optical/electronic properties (2, 3, 16), simply by manipulating the order and thickness of the organic/inorganic components (28). Combining small molecule organic or polymers with early transition metal oxides should yield novel and synergistic electro-optical properties and bioactive surfaces (29−31).

From the "inorganic" point of view, Si- and Ti-based materials, with their tunable refractive indices, can be incorporated within thin film architectures through a sol−gel process and provide a predictable dielectric response (32, 33). On the other hand, V- and W-based oxides can display electrochromic behavior and their manipulation at the nanoscale can afford interesting structure−property relationships. For example, by using the LbL method, Huguenin et al. fabricated V_2O_5-poly(aniline) nanocomposites possessing *both* the electrochemical profile of the inorganic oxide *and* the chromogenic properties of the organic polymer (33). Not only did the metal oxide layers induced dimensional ordering, high mechanical stability and carrier mobility were also observed with improved processing conditions.

* To whom correspondence should be addressed. E-mail: radvincula@uh.edu.
Received for review September 12, 2010 and accepted October 29, 2010

DOI: 10.1021/am100867q

Published on Web 11/16/2010

On the other hand, from the "organic" point of view, the use of π-conjugated and conducting polymers (CPs) provides for a vast class of processable organic semiconductors whose tunable optical/electronic emission/absorption varies with chemical or electrochemical doping (34, 35). Within the realm of such CPs, carbazole-based polymers are well-known electro-optically active materials for their hole-transporting (36) and electroluminescent properties (37, 38). Indeed, they have found practical applications as electro-optical devices (39), light-emitting diodes (40, 41), and polymer-based batteries. Through a conjugated polymer precursor route, cyclic voltammetry (CV) allows extensive cross-linking of carbazole units via anodic electrochemical oxidation (42−44). The outcome is a conjugated polymer network (CPN) film or pattern on a substrate (45−52). The in situ characterization of this process has been realized with surface sensitive analytical techniques such as electrochemical surface plasmon resonance (EC-SPR) (53, 54) and quartz crystal microbalance (E-QCM) as previously demonstrated by our group (55, 56). For precursor polymers, both single and mixed pendant electroactive groups can be utilized (55−59). Smooth morphologies and high-optical quality films have been realized in such CPN films which have found applications in organic light emitting diode (OLED) devices (42, 43). The characterization of such precursor films by electrochemical impedance spectroscopy (EIS) has recently been demonstrated (60). It utilizes a sweeping voltage which is applied to the film and can be utilized as a diagnostic method for anticorrosion coatings. The information obtained includes redox characteristics, conducting/insulating features, and coating stability which can be modeled. Thus, an extensive electrochemically cross-linked film can be achieved by a rational precursor polymer design whose electropolymerizable side groups can be connected by electrochemical CV or potentiostatic methods.

In this work, we fabricated nanostructured hybrid organic−inorganic ultrathin films on several substrates (quartz; gold; tin-doped indium oxide, ITO) based on a combined LbL electrostatic assembly and surface sol−gel layering protocol of alternating polyelectrolyte polycarbazole precursors and TiO_x layers, respectively. Subsequently, the polyelectrolyte layers were electropolymerized as CPN layers. The polyelectrolyte precursors are composed of alternate layers of poly[2-(*N*-carbazolyl)ethyl methacrylate-co-methacrylic acid] (PCEMMA) (−) and a random copolymer, poly[2-(9*H*-carbazol-9-yl)ethylmethacrylate]-co-[2-(methacryloyloxy)-*N*,*N*,*N*-trimethylethanaminium] iodide (CCP) (+) deposited through the LbL technique (Figure 1). The $Ti(OBu)_4$ sol−gel layers were intercalated every 2.5 polyanion/polycation layers. PCEMMA is a copolymer that was utilized in its deprotonated form while the CCP is a random polymer bearing a quaternary ammonium group. Both species have pendant carbazole electroactive units. The interest is in enabling a nanostructured stacking procedure resulting in confined electrochemical cross-linking of the precursor carbazole derivatives intercalated within inorganic oxide layers. We emphasize the use of the LbL self-assembly in order to observe

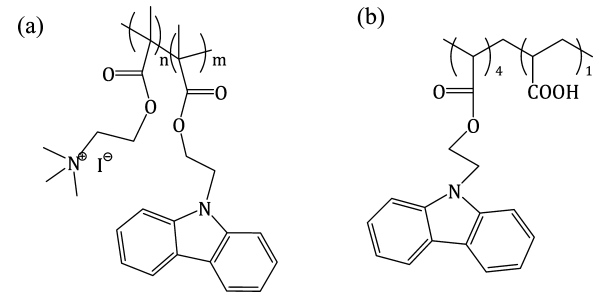

FIGURE 1. Chemical structures of (a) poly[2-(9*H*-carbazol-9-yl)ethylmethacrylate]-co-[2-(methacryloyloxy)-*N*,*N*,*N*-trimethylethanaminium] iodide, CCP (+), a random copolymer, and (b) poly [2-(N-carbazolyl) ethyl methacrylate-co-acrylic acid], PCEMMA, (−) used for the LbL self-assembly method.

quantitative electrochemical CPN formation in morphologically defined ultrathin films (48, 49).

The surface sol−gel process as developed by Kunitake et al. is a relatively simple method that allows deposition of oxo-hydroxo materials in an LbL manner as well (8, 24, 25). The process, with its alternating chemisorption-hydrolysis steps, is a suitable method of intercalating a dielectric layer within nanostructured architectures because the film thickness can be controlled similarly at the nanoscale level. The whole LbL/sol−gel process is represented in Scheme 1.

UV−vis absorption spectroscopy, quartz crystal microbalance - with dissipation monitoring (QCM-*D*), and null ellipsometry were utilized to monitor and characterize ultrathin film growth. Shown also in Scheme 1 is the anodic oxidation of the carbazole side groups via CV within the PCEMMA/CCP layers. Fluorescence and UV−vis spectroscopy confirmed the occurrence of cross-linking. Further investigation of such hybrid films may show viability as hole-transport/electron blocking materials in OLEDs (61, 62) (i.e., a spatially defined gradient layers), novel dielectric mirrors (63), and enhanced heterojunction photovoltaic devices (64).

EXPERIMENTAL SECTION

Materials. All the reagents were used as received unless otherwise stated. 2,2′-Azobisisobutyronitrile (AIBN; Aldrich, 98%), absolute ethanol (EtOH), and dimethylsulfoxide (DMSO) were utilized without further purification. Toluene, triethylamine (TEA) and tetrahydrofuran (THF) were distilled before using according to the normal laboratory procedures. 11-Mercaptoundecanoic acid (Aldrich, 95%) was used for functionalizing the Au-coated QCM crystal. Functionalization of the silicon wafers, quartz slides and ITO glasses was carried out with 3-aminopropyltrimethoxysilane (APS; Acros, 95%). CCP and PCEMMA were synthesized in the laboratory and the synthesis of PCEMMA has been previously reported (65). 10^{-2} M solutions of $Ti(OBu)_4$ were prepared by dissolving 341 μL of $Ti(OBu)_4$ (Alfa Aesar, 99.9%) into 100 mL of toluene/EtOH (1/1, v/v). CCP solutions were prepared by dissolving 40 mg of polyelectrolyte in 25 mL of deionized water (resistance = 18.2 MΩ), followed by dropwise addition of 25 mL of DMSO and then sonication (30 to 45 min.); no p*H* adjustment was required. PCEMMA solutions were prepared by dissolving 40 mg of polyelectrolyte in 50 mL of deionized water/DMSO (2/3, v/v), followed by dropwise addition of 0.1 M $NaHCO_{3(aq)}$ to adjust the pH to 8 and subsequent sonication (45−60 min.).

Synthesis of N-[3-(Dimethylamino)propyl]methacrylamide, Cationic Monomer (1). In a 500 mL round-bottomed flask, 8.48

Scheme 1. Schematic Description of Surface Modification (a), Multilayer Deposition (b), Surface Sol-Gel LbL Process (c) On a Substrate Surface (Si, quartz, ITO, Au), and (d) CV-Induced Electropolymerization of the Electroactive Units in CCP (Blue) and PCEMMA (Red)

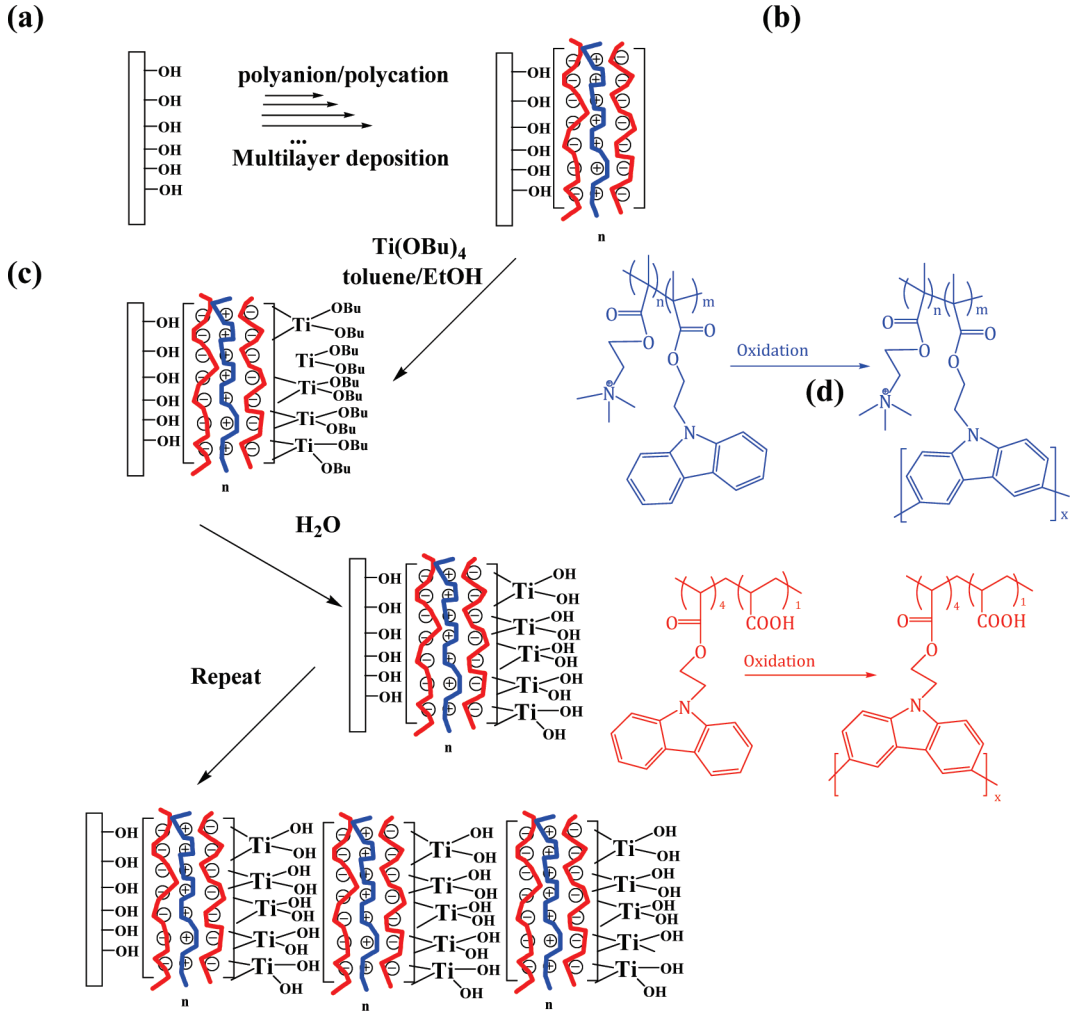

mL (122 mmol) of TEA was added to 10.0 g (97.8 mmol) of 3-(dimethylamino)propylamine dissolved in 25 mL of dry THF. The reaction mixture was stirred at room temperature for 5 min and then in an ice bath at 0 °C. 6.39 g (122 mmol) of methacryloylchloride in 75 mL of dry THF was added dropwise to the cooled solution over a period of 1 h under a N_2 atmosphere. After the addition had been completed, the reaction mixture was allowed to react at 0 °C for 5 min and then was left stirring at RT for an additional 12 h. Triethylammonium salt was filtered out, and the filtrate was dried under vacuum to remove the solvent. The purified yellowish liquid was stored in a refrigerator until further use. ^{1}H NMR (300 MHz, $CDCl_3$) δ (ppm): 5.78 (d, 1H), 5.36 (d, 1H), 3.47 (m, 2H), 2.53 (t, 2H), 2.35 (s, 6H), 1.98 (s, 3H), 1.76 (m, 2H).

Synthesis of 2-(9H-Carbazol-9-yl)ethyl Methacrylate (2). In a 100 mL round-bottomed flask, 2.00 g (9.46 mmol) of 2-(9*H*-carbazol-9-yl)ethanol was dissolved in 25 mL of dry THF. One gram (9.56 mmol) of methacryloyl chloride was dissolved in 10 mL of dry THF into an addition funnel. The methacryloyl chloride solution was added to 2-(9*H*-carbazol-9-yl) ethanol at 0 °C dropwise and then allowed to warm to room temperature overnight. The solvent was removed in vacuum and the product was purified via column chromatography. Product yield: 50% (1.58 g). ^{1}H NMR (300 MHz, $CDCl_3$) δ (ppm): 8.10 (d, 2H), 7.49 (m, 4H), 7.26 (m, 2H), 5.92 (s, 1H), 5.47 (s, 1H), 4.61 (t, 2H), 4.53 (t, 2H), 1.80 (s, 3H).

Polymerization and Quaternization of Cationic Carbazole Polymer (3, CCP). One gram (3.60 mmol) of carbazole methacrylate, 2.4 g (14.4 mmol) of methacrylamide monomer, and 50 mg (8.20 mmol) of AIBN were dissolved in 20 mL of dry THF and charged in a Schlenk flask. The reaction mixture was subjected to 3−4 freeze−pump−thaw cycles to remove any trace of gases prior to being placed in a constant oil bath at 60 °C for 12 h. After polymerization, 1.3 g (9.0 mmol) of methyl iodide was added to the Schlenk flask, the reaction mixture was diluted to 50 mL with the addition of water and left to stir for 2 days. After 2 days, the polymer was precipitated from acetone and dried in the vacuum oven for 24 h. ^{1}H NMR (300 MHz, DMSO-d_6) δ(ppm): 8.17 (br, 2H), 7.51 (br, 4H), 7.24 (br, 2H), 3.9−3.4 (m, 8H), 3.4−2.8 (br, 15H). FT-IR (KBr, cm^{-1}): 1167 (m, C−O−C), 1462 (s, C−O−C), 1481 (s, C═C), 1597 (m, C═C), 1635 (m, C═C), 1724 (vs, C═O), 2954 (m, C−H), 3005 (w, C−H). GPC: $\bar{M}_n$ = 9059, $\bar{M}_w$ = 12457, $\bar{M}_w/\bar{M}_n$ = PDI = 1.375. The overall synthetic route is depicted in Scheme 2.

Instrumentation. All the measurements were recorded at room temperature unless otherwise stated. NMR spectra were collected on a General Electric QE300 spectrometer (^{1}H 300 MHz) with tetramethylsilane (TMS) as internal standard. UV−vis and fluorescence spectra were recorded on a HP-8453 UV−vis spectrometer (within the 250−700 nm range) and a Perkin-Elmer LS50B spectrometer, respectively. QCM-*D* experiments were performed on a KSV QCM-Z500 (Biolin Scientific) system

Scheme 2. Schemes for the Synthesis of Poly[2-(9*H*-carbazol-9-yl)ethylmethacrylate]-co-[2-(methacryloyloxy)-*N*,*N*,*N*-trimethylethanaminium] Iodide (CCP)

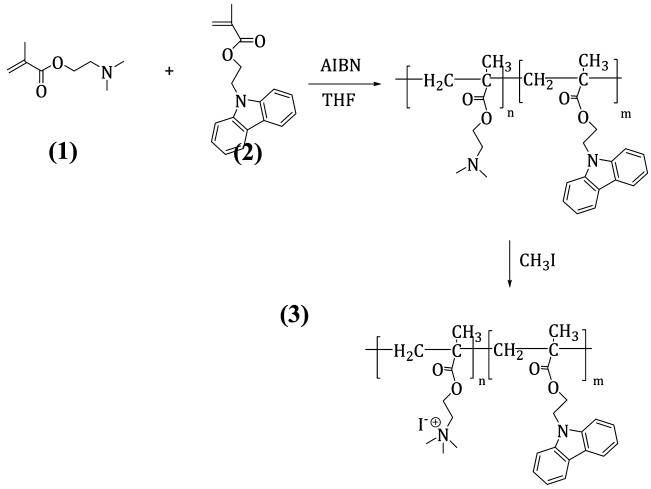

equipped with Au-coated quartz crystals ($f = 5$ MHz, frequency resolution 10^{-2} Hz, mass resolution 1.77×10^{-9} cm^{-2} in liquid, D sensitivity $\approx$. 3×10^{-8} in liquid). Null ellipsometry was performed using an Optrel GmbR Multiskop at 60° incidence and a 632.8-nm He−Ne light source. CV and potentiostatic measurements were executed using a one-compartment, three-electrode cell driven by Princeton Applied Research Parstat 2263 instrument and AMEL instrument potentiostat (model 2049).

Surface Activation. Silicon wafers (N100 type) were cut into 1 × 2 cm squares, sonicated in Millipore water (15 min.), acetone (5 min.), Millipore water again (5 min.) then soaked in piranha solution (**Caution***: strong oxidizer!*), 30% H_2O_2/conc. H_2SO_4 (3/7, vol/vol) for 60 min. They were then thoroughly rinsed with Millipore water, dried under N_2 stream and plasma-cleaned for 3 min. The activated surfaces were dried in oven (45 min.) and functionalized by dip-coating in APS solution (0.5% v/v in toluene) for 30 min at 70 °C in a staining jar. Fresh toluene was added for subsequent sonication (15 min.), followed by final drying under N_2 stream. The substrates were stored in 0.1 M HCl until needed. This procedure affords a positively charged surface onto the solid support. Flat ITO-coated glasses were sonicated in isopropanol (10 min), hexane (10 min), and toluene (10 min). Subsequent plasma-cleaning (2 min) yielded activated surfaces that were functionalized by dip-coating in APS solution (0.5% v/v toluene, Teflon-taped staining jar) for 30 min at 50 °C, sonicated in fresh toluene (15 min) and finally dried under N_2 stream. The gold-coated QCM resonator and glass slides were rinsed with Millipore water, dried under N_2 stream, plasma-cleaned (3 min), and then soaked in $NH_3/H_2O_2/H_2O$ solution (1/1/5, v/v) for 10 min. Subsequent rinse with Millipore water, drying under N_2 stream and plasma-cleaning (3 min) yielded clean gold surfaces that were finally dipped overnight in a solution of 11-mercaptoundecanoic acid in EtOH (1 mg/mL, 95% activation).

LbL Deposition. The fabrication of the [PCEMMA/(CCP/PCEMMA)$_2$/TiO$_x$]$_n$ thin films was realized by hand dipping of all substrates as follows. An APS-activated substrate (either silicon, ITO, or quartz) was alternatively immersed in PCEMMA/CCP solutions (15 min each, chemisorption steps), DI water (circa 20 s, rinse step), Ti(OBu)$_4$ solution (10 min, chemisorption step), and toluene/EtOH (few seconds, rinse step) to remove the excess of alkoxide. The as-activated surface was then driven to complete hydrolysis of Ti-based layer by immersion in DI water (2 min). The PCEMMA/CCP bilayers were assembled twice before the deposition of the TiO$_x$ sol−gel and the whole procedure was repeated twice; conclusive, topmost (CCP/PCEMMA)$_2$ layers were then deposited. Thus, the resulting film architecture can be described as [A/B/A/B/A/C]$_2$/A/B/A/B/A (A = PCEMMA, B = CCP, C = TiO$_x$). No pH adjustment was made.

QCM *D* Measurements. All the measurements were recorded at 20.0 ± 0.1 °C. QCM is a mass-sensitive, mechanical-based surface technique: when a piezoelectric quartz crystal is excited by an applied voltage, it oscillates at its fundamental frequency f_q. A small mass applied onto the QCM crystal results in a change, Δf, of this frequency. Once the mass is deposited, a shear wave dissipates through the crystal; the piezoelectric effect can be detected and electrically amplified. The crystal is driven at its resonance frequency, and then the electrical circuit is switched off so that the amplitude of such decay can be monitored. Both the resonance frequency f and the dissipation D of the oscillating crystal can be measured. The former quantity is related to the mass deposited while the latter one describes the rigidity and viscoelastic features of the film. D indicates how purely elastic the crystal oscillation is (66): its change, ΔD, is a measure of the dampening of the system being loaded. In order to investigate the viscoelastic behavior of the overall film and evaluate the effect of the intercalation of inorganic slabs, we monitored the in situ fabrication of the (PCEMMA/CCP/TiO$_x$)$_n$ film and its "purely organic", counterpart, a (PCEMMA/CCP)$_n$ LbL film, namely, with no intercalation of TiO$_x$ layers. The sequence of the material injection into the QCM chamber followed the same scheme (in terms of deposition sequence, absorption time and rinse steps) as reported for the LbL deposition.

Electrochemical Cross-linking. Cyclic Voltammetry (CV) was utilized for electro-polymerization and cross-linking of the carbazole groups within the organic moieties. The working electrode was an ITO-coated glass substrate which the films were fabricated on; a platinum wire and Ag/Ag$^+$ electrode (10^{-2} M in CH_3CN) were utilized as counter and reference electrodes, respectively. 10^{-1} M tetrabutylammonium hexafluorophosphate [Bu$_4$N][PF$_6$] or TBAH in dry CH_2Cl_2 was used as supporting electrolyte along with the cyclic potential sweep technique over the 0 to 1.4 V range (scan rate: 50 mV s^{-1}). The thin films were dried in a vacuum oven overnight at 50 °C prior to effectuating CV to remove excess solvents.

RESULTS AND DISCUSSION

Synthesis and Film Characterization. PCEMMA and CCP are carbazole-bearing, water-soluble polyelectrolytes (anionic the former, cationic the latter) compatible with LbL self-assembly and sol−gel processes. They are also precursors for the formation of polycarbazole by chemical oxidative or electrochemical polymerization (45−52, 55, 56). In particular, CCP was obtained from free radical polymerization, with M_w = 12457 g/mol and PDI = 1.375. The presence of carbazole units on both oppositely charged polyelectrolytes is important since they enable a high density of electrochemically cross-linkable groups to form CPN (48, 49). We have demonstrated the quantitative electropolymerization of such polyelectrolyte polycarbazole precursors (48) and their electronanopatterning using conducting atomic force microscopy (CS-AFM) (49).

The films were then deposited by LbL. A steady, linear layer deposition was realized on all of the rigid support substrates utilized for the CCP/PCEMMA/TiO$_x$ ultrathin films. Overlays of the UV−vis spectra for the LbL assembly, recorded after every single deposition on quartz plate are shown in Figure 2.

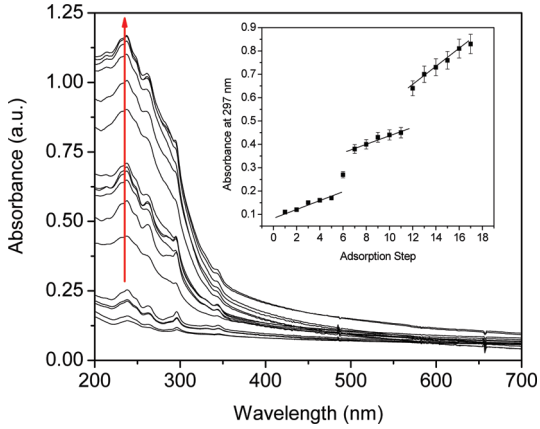

FIGURE 2. UV−vis spectra of PCEMMA/CCP/TiO_x multilayer films and absorbance increment (inset, $\lambda = 297$ nm) per layer plotted as a function of deposited layer.

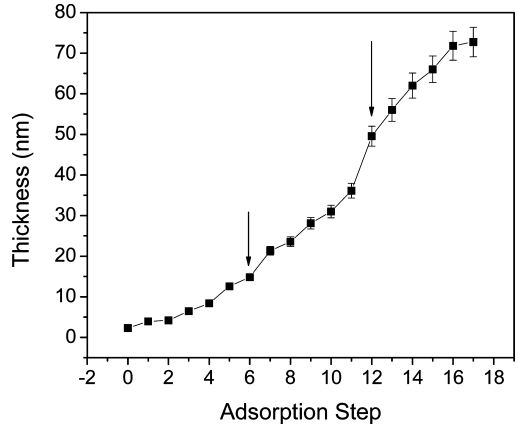

FIGURE 3. Thickness increment per layer deposition obtained from null ellipsometry (incident angle: 60°, refractive index: 2.00). The two TiO_x depositions are indicated by the arrows.

The bands at 265 and 297 nm are attributable to the $\pi-\pi^*$ transitions within the carbazole groups (67). These absorption peaks increase as the carbazole concentration increases, according to the Beer−Lambert law, a typical behavior in an LbL deposition. Comparison with our previous work showed a steeper absorbance increase at λ_{max}= 297 nm, most likely due to the presence of oxide networks arising from the sol−gel process (68−70). Indeed, the use of TiO_x-based slabs sandwiched between conjugated polymers affects the architecture and electro-optical behavior of such thin films (vide infra). This is further confirmed by plotting the absorbance versus the number of the deposited polyelectrolyte layer pairs (inset in Figure 2). Although TiO_2-based thin films do not affect the UV attenuation coefficient of carbazole species (e.g., poly(*N*-vinylcarbazole), PVK) (69, 70), even when the thickness of the polymer layer is comparable, the largest absorbance increases here were observed as a step-function after sol−gel depositions; in other words, the TiO_x slabs have less UV-transparency than the polyelectrolyte layers in the composite film.

Likewise, the optical thickness determined by ellipsometry showed an upward, pseudolinear behavior (Figure 3). The film thickness was measured after every deposition and, again, is characterized by the "jumps" corresponding to the TiO_x depositions (indicated by the two arrows). The thicknesses at these junctions were determined to be 2.20 and 13.4 nm, respectively. This difference may also be due to the total increase of the number of polyelectrolyte-based layers and concomitant film swelling by aqueous solvent because of the prolonged LbL process. The resulting effect is that the effective hydrolysis of $Ti(OBu)_4$ molecular precursors and subsequent sol−gel deposition favors the formation of thicker films at the latter stages. The choice of butoxide over other alkoxides was due to the fact that it showed easier workability with the solvent and reasonably smooth film deposition (32, 33).

In Situ QCM-*D* Studies. QCM measurements were also utilized to monitor the in situ depositions of single PCEMMA, CCP, and TiO_x layers. In general, each step resulted in an increase of the associated frequency shifts of the QCM crystal but the plot was not included in this paper because of experimental limitations working with toluene (deposition with TiO_x). However, previous plots of similar step absorption monitoring with QCM has been demonstrated (48). If the depositions are done in vacuum or air, the mass-frequency relationship can be quantitatively expressed through the Sauerbrey equation (71, 72). The characteristic deposition kinetic curves for PCEMMA, CCP and TiO_x in the hybrid thin films are shown in Figure 4, plots a, b, and c. The most straightforward data obtainable from QCM measurements is a mass value (in the nanogram range) per unit area (the Au electrode). The microbalance per se does *not* directly measure mass but must satisfy the Sauerbrey equation (71). For this to hold, the deposited layer must be rigid, thin, and homogeneous and no viscous losses/viscoelastic effects of the solvent must be present. In other words, only uniform, rigid, thin-film deposits can fully couple with the crystal oscillation (73, 74). In air, viscoelastic effects can be neglected, whereas this is not clearly possible in liquids because a viscous solvent exerts a stress sideways on the topmost film surface and this effect scales linearly with the mass. This is even more pronounced if polyelectrolytes are being deposited, because they trap water inside their loops and tails (25). The Δf is dependent upon the total oscillating mass which can include the solvent coupled to the adsorbed layers. Because of the aforementioned reasons, dissipation monitoring (QCM *D*) is a better technique for analyzing more complex viscoelastic systems (72). The dissipation factor, *D*, may be expressed as

$$D = \frac{E_d}{2\pi E_s} \quad (1)$$

E_d and E_s are the energy dissipated and stored during the decay, respectively. An important consequence is that, for the Sauerbrey equation to be valid, no change in dissipation must be detected, namely $\Delta D = 0$. For rigidly bound species, this will be true. For viscoelastic species, however, E_d through a layer will increase. Dissipation monitoring can therefore shed light on these ambiguities because a qualitative measure of the relative stiffness of a layer can be inferred (25). As previously stated, we set out to evaluate the effect of the

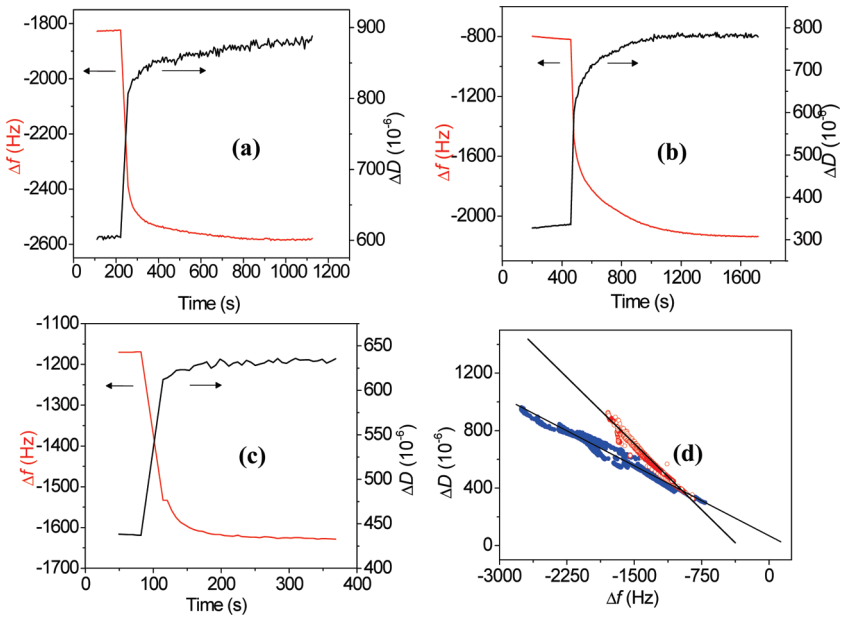

FIGURE 4. Typical $\Delta f/\Delta D$ vs time depositions of TiO_x (a), CCP (b), and PCEMMA (c). Plot d: Dissipation shifts (ΔD) versus frequency shifts (Δf) for PCEMMA/CCP/TiO_x (blue) and PCEMMA/CCP (red) multilayer films, 3rd harmonic overtone plotted.

intercalated inorganic slabs in the LbL film. Although the ultimate goal was the evaluation of the electroactivity of the carbazole-bearing polyelectrolytes, it is important to characterize the hybrid property of combining the organic and inorganic material. In order to do so, we first needed to comprehend the salient features of the simpler, organic PCEMMA/CCP film deposition in terms of viscoelastic behavior. Comparative ΔD versus Δf plots of $[PCEMMA/CCP/TiO_x]_n$ and $(PCEMMA/CCP)_n$ thin films indicated that the swollen, more viscous film was actually the one *with* the inorganic slabs (Figure 4d). The calculated $\Delta D/\Delta f$ slopes were 0.45 (PCEMMA/CCP film) and 0.32 (hybrid film), respectively.

The chemisorption of $Ti(OBu)_4$, followed by hydrolysis, produced the oxy-hydroxy-Ti xerogel; this allowed for H-bonding/entrapment of small molecules (BuOH, H_2O) within the as-formed oxide framework. A look at ΔD for PCEMMA, CCP and TiO_x shows dramatically higher values, up to 5×10^{-4}. The simultaneous presence of polyelectrolytes and a xerogel introduces more swelling-related issues: whenever there is solvent entrapment in a textured architecture, the deviations from the Sauerbrey-like behavior are more likely to occur. In particular, the relationship is no longer valid for a viscoelastic polymer in water (typical Newtonian liquid). Several models have been brought up and discussed previously (75−77). Some have pointed out that, for hydrated polymer films, there is a minimum thickness (at which significant deviations arise) that *increases* as the film viscosity *increases*: the more imbibed a film is, the thicker it becomes. Sensibly higher dissipation values ($>5 \times 10^{-6}$) are indicative of non-Sauerbrey behavior (46, 78, 79). Indeed, if polyelectrolytes are deposited, the layer will always contain such species as well as imbibed water. Apart from the obvious contribution of solvents within the polyelectrolyte layers, the presence of solvents inside the TiO_x slabs as well conferred pronounced viscoelastic behavior to the structure. Therefore, the outer layers seem to be not as well coupled

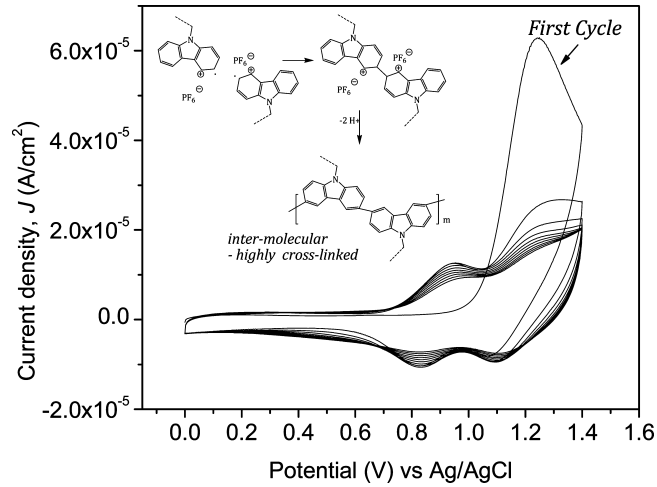

FIGURE 5. CV traces of the polymerization within $[(PCEMMA/CCP/TiO_x]_n$ multilayered, hybrid film (10 cycles). Electrolyte: 0.1 M $[Bu_4N][PF_6]$ or TBAH in CH_2Cl_2. Potential window: 0−1.4 V, scan rate: 50 mV s^{-1}.

to the quartz surface as initially thought. The direct application of the Sauerbrey equation therefore becomes questionable because of the dissipation values, which represent a clear underestimation of the solvent inclusion in both systems (24, 25, 78).

Electrochemistry. Electrochemical properties in LbL films have long been of high interest not only for applications in sensing but also to relate their nanostructure with electrochemical phenomena in structure−property relationships (99−101). Shown in Figure 5 is the cyclic voltammogram of the composite $[PCEMMA/CCP/TiO_x]_n$ film. Electropolymerization converts the precursor polymers the PCEMMA/CCP layers into CPN films containing both inter- and intramolecular cross-linkages between the pendant carbazole units (55, 56). The onset of the irreversible first scan (~1.10 V vs Ag/AgCl) is the anodic oxidation potential, that is, the formation of carbazolyl cation radicals and subsequent start

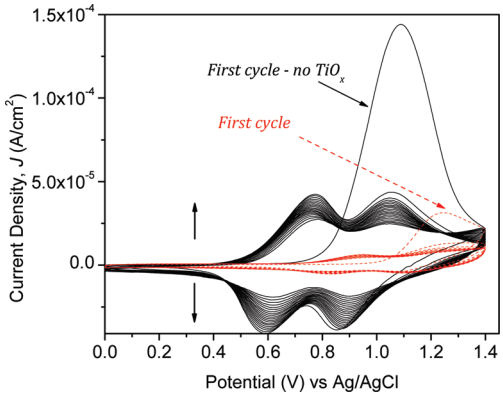

FIGURE 6. Comparison of CV scans for ultrathin films with (red, dashed lines) and without (black, solid lines) TiO_x slabs, 20 cycles. Electrolyte: 0.1 M TBAP in CH_2Cl_2. Potential window: 0−1.4 V scan rate: 50 mV s^{-1}.

of electropolymerization of the precursor polymers by the carbazole groups (82−91). Cross-linking in this case is a process that occurs as a three-electron transfer and dimerization of pendant carbazole ring via the 3,6-positions. This in turn leads to intermolecular cross-linking (Figure 5 inset) and increase in conjugation length (92, 93). Progressively developing quasi-reversible CV traces (2nd cycle and up) showed lower oxidation potentials (onsets at 0.80 and 1.00 V) and their corresponding reduction potentials (1.00 and 1.20 V). In all the cases, the anodic current appeared to increase as subsequent cycles, namely further cross-linking, occurred; lower oxidation potentials and doping/dedoping cycles could be observed.

Striking features of this system, however, arise from the interplay of organic and inorganic moieties: the current response of the composite film showed dramatic changes when the inorganic framework was absent (Figure 6). Moreover, the aforementioned CV scans yielded two oxidation/reduction peaks instead of the canonical one peak in carbazole monomers and polyvinylcarbazole (PVK) (37, 88, 90, 91). First, the two redox peaks appear whether or not TiO_x is present (see below): this suggests that they do not come from electrochemical activity of the inorganic oxide. A few carbazole-based systems have shown this electrochemical feature (65, 94−98). In as much as a previous report of ours made use of the same starting material (PCEMMA) (65), we initially invoke a majority 3,6-connectivity of the carbazole side groups during the electrochemical cross-linking, with the second set of redox waves attributable to further oxidation to different types of carbazolyl cation species, majority of which should be the dication or bicarbazylium cations (two electron process). However, such pair of redox peaks bears close resemblance to the CV traces reported by Marrec et al. and Pelous et al. (97, 98). Moreover, Cattarin et al. observed such a behavior in $HClO_4$ solutions of N-substituted carbazole monomers when the potential range was widened from 0.85 to 0.90 up to 1.1 V (95). They also noted some film degradation in the cross-linking of *N*-phenyl carbazole, when the window was widened to 1.25 V, as well as other C−C coupling products. They claimed these results to be due to oligomerization (at least tetramers), as indicated by ESR activity and conductivity measurements. According to Siove (96) and Pelous (97), these two redox peaks may be assigned to one- *and* two-electron oxidation of a carbazolyl unit, leading to cationic *and* dicationic forms. However, Marrec's starting materials were polyethers bearing *two* carbazole groups. Therefore, they invoked their simultaneous presence to afford two different, possible electropolymerization processes after the dimer formation: a two-electron and a four-electron process. These, in turn, would lead to polymer fragments and electronic conducting "islets", although they also pointed out that the latter one was unlikely to occur.

Solution-type electropolymerization typically generates one oxidation/reduction peak. However, in such cases, the potential window is kept below 1.00 V. We deliberately chose a wider range in order to avoid film dissolution and elicit film deposition. The upper switching potential (1.4 V) did not influence the polyelectrolyte responses and allowed us to rule out anodic decomposition. There is also the possibility of coupling at different positions within the carbazole rings in that the two peak pairs may indicate both 3,6- and 2,7-linking, the latter one being more unlikely, on the basis of position activations within the benzene rings and electron density. From this viewpoint, our electrochemical cross-linking afforded a system whose behavior resembled the ones described by Iraqi (88) and Zotti (102).

Also, the CV carried out on the ultrathin film without TiO_x slabs showed more pronounced current intensities (J values up to $\sim 10^{-4}$ A cm^{-2}, Figure 6, black, solid lines). The onset oxidation potential shifted to a lower value (0.69 V) and the two growing redox peaks were found much more distinct in this case. The different extension at which cross-linking occurs can be clearly evaluated by overlapping the two CV traces. Comparison of these anodic currents with similar works (37, 45, 102) allows us to place this system halfway between a more efficient (Iraqi's work, $I \approx 10^{-3}$ A) and less-efficient (Inzelt and Xia's works, $I \approx 10^{-5}$ and 10^{-6} A, respectively) doping/dedoping cycles of carbazole-based polymers. Our current peaks are in the 10^{-4}−10^{-5} A range, which seems to be a common value for solution-cast/LbL films (48, 49). The higher current for the same thickness indicates that nearly all of the carbazole units are electropolymerized up to saturation, whereas this is not the case in the presence of the blocking TiO_x layers. This also means that an LbL structure is more efficient compared to simple cast films or electrodeposition (electropolymerization) of monomers from solution (82). A similar phenomenon on improved efficiency and lower oxidation potential has been detected using different media or micellar surfactants (111). This was also observed for thiophene and benzene derivatives in strong acidic medium, which may be due to the formation of π-complexes between the aromatic ring the and the H^+ or cation which decreases the oxidation potential (112). In the case of these films, an analogous effect may be occurring in the presence of the tethered-$N^+(CH_3)_3$ in the CCP main-chain. This is in fact consistent with a lower oxidation potential for similarly prepared LbL films of PCEMMA and poly[4-(9*H*-carbazol-9-yl)-*N*-butyl-4-vinylpyridinium

Table 1. Relevant Electrochemical Data of the Two Different Film Architectures[a]

hybrid film	PCEMMA/CCP film	
onset (V)	0.87	0.68
E_{pa1} (V)	0.94	0.77
i_{p1} (mA)	$1.28 \times 10{-}5$	6.90×10^{-5}
E_{pa2} (V)	1.28	1.04
i_{p2} (mA)	$2.65 \times 10{-}5$	7.01×10^{-5}
E_{pc1} (V)	0.83	0.60
i_{pc1} (mA)	$-1.09 \times 10{-}5$	-6.04×10^{-5}
E_{pc2} (V)	1.09	0.88
i_{pc2} (mA)	$-9.64 \times 10{-}6$	-5.72×10^{-5}
ΔE_1 (V)	0.11	0.17
ΔE_2 (V)	0.19	0.17

[a] Shown are anodic and cathodic current/potentials E_{pa}, E_{pc}, i_p, i_{pc}. Both redox peaks (1 = lower potential, 2 = higher potential) are reported.

bromide] (P4VPCBZ) or PCEMMA/P4VPCBZ on a previous report (49). Thus, a confined and "self-acidified" LbL film electropolymerization enables a more efficient electrochemical polymerization of the carbazole units since it decreases the applied potential necessary for the electropolymerization. It also increases the thermodynamic oxidation potential of the whole film which leads to broaden the domain of electroactivity in the oxidation process. It is possible to revisit the role and transport of the TBAH counterion by using other sizes or charge density with this LbL films (113). A comparison on the significant electrochemical data of the two different film architectures (with and without TiO_x) is presented in Table 1.

The presence of TiO_x slabs clearly affects the current response, in that the inorganic oxide acted as a current blocker and dielectric material, attenuating extensive electropolymerization, and the doping−dedoping cycles across the film. One possible role is in limiting the transport of the electrolyte counterions, TBAH, across the film either through a decrease in diffusion kinetics or adsorption on the −OH groups of the TiO_x matrix layer. This may be mitigated by the presence of the cationic $-N^+(CH_3)_3$ in the polymer backbone of CCP. The blocking effect of the TiO_x layer may also be seen as insulating in behavior because it causes the conductivity to be less from the surface, rendering a "delayed" oxidation, hence the higher anodic oxidation potential in the hybrid film or higher resistance, that is, increase in heterogeneous electron-transfer kinetics, IR drop of the film ($V_{total} = V_{across\ film} + I[R_{film} + R_{soln}]$) (114). Tan et al. reported the same insulating/poor conducting nature of a similar gel structure (103). According to their work, successive functionalization of Ti-based xerogels with protoporphyrin and ferrocene carboxylic acid (FCA) enabled better photoactivity and electron transfer capabilities.

An important parameter concerning conducting polymers is the doping level γ, corresponding to the number of electron exchanged per aromatic ring. It can be easily determined electrochemically from the following equation:

$$\gamma = 2/([Q_i/Q_f] - 1) \quad (2)$$

where Q_i is the charge density required for the electrodeposition of the film and Q_f is the faradic charge density recorded during the oxidation of the film. From this relationship, it is obvious based in Figure 6 that γ for $[PCEMMA/CCP]_n > [PCEMMA/CCP/TiO_x]_n$

Another interesting point to note is the possible change in the band gap energy in the presence of the TiO_x slabs. This will be of interest in considering possible applications of such films in junction sandwich devices such as OLEDs. Because electrodes prepared with LbL films exhibit high electrochemical stability, it is possible to combine UV−vis spectroscopy and electrochemistry to estimate the energy level diagram of the electropolymerized material (48, 49). For example, the band gap energy (E_g), ionization potential (IP), and electronic affinity (EA) can be determined based on the CV (usually with respect to the highest occupied molecular orbital (HOMO) level of −4.8 eV for the ferrocene/ferrocenium redox system). The onset potentials (E') of the LbL films can be estimated from the intersection between the two slopes drawn at the rising oxidation (or reduction) current and background current in the CV. The oxidative potential can be directly related to the IP of the electrochemically active film, while E_g and EA can be obtained from the UV−vis spectra and CV, respectively.

To have an appreciation of the E_g differentiation, it is necessary to review the nature of charge injection mechanism in the forward direction (ITO positive) and its implications on a space-charge limited current (SCLC) conditions. In most cases, the Fowler−Nordheim model has been found to be applicable in the high field domain, which presumes tunneling of charge carriers directly into the bands of the semiconductor (115). According to the Fowler−Nordheim model the current density can be expressed as

$$j = \left(\frac{J_0 F^2}{\phi}\right)\exp\left[\frac{K\phi^{3/2}}{F}\right] \quad (3)$$

where $F = V/d$ is the applied field (d is the thickness of the PVK film), J_0 the prefactor, K is a constant, and ϕ is the energy barrier height. A general mechanism for OLED operation is by double injection of electrons and holes from the electrodes, followed by formation of excitons, whose radiative decay results in light emission. Holes being the majority carrier determine the I−V characteristics while the EL characteristics are determined by the electron minority carrier injection. For instance, high EA (n-type) conjugated polymers improves electron injection/transport and low IP (p-type) conjugated polymers improves hole injection/transport. Regulating the ITO/dielectric layer interface therefore, plays an important role in OLED performance primarily through band-bending at the HOMO level. Consider a typical ITO/PVK/Al junction device. The HOMO and the lowest unoccupied molecular orbital (LUMO) of the PVK are 5.7 and 2.2 eV, respectively (116, 117), the EA of the ITO is about

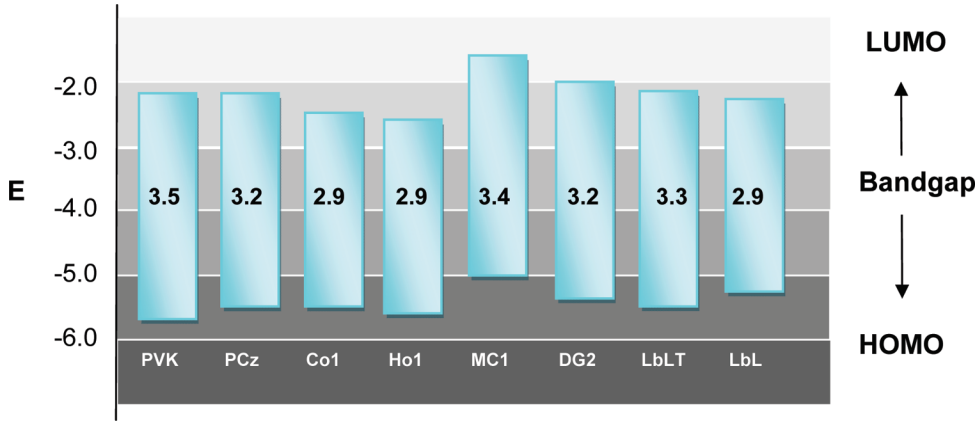

FIGURE 7. Summary of the bandgap energy, E_g in eV of various polycarbazole derivatives in comparison to the [PCEMMA/CCP/TiO$_x$]$_n$ (LbLT) and [PCEMMA/CCP/TiO$_x$]$_n$ (LbL) films.

4.8 eV, while the work function of Al is 4.25 eV. Therefore, the whole energy barrier at the ITO/PVK interface is about 0.9 eV, while the electron energy barrier at the PVK/Al interface is around 2 eV. The smallest barrier height is situated at the ITO/PVK interface and therefore holes are the majority carriers crossing the device. Therefore, it is important to focus on the energy barrier, which controls the hole injection energy, ϕ, of the ITO/PVK interface (42, 43).

A summary of the energy levels of various carbazole and polycarbazole thin film derivatives in relation to the LbL films are shown in Figure 7. For polycarbazole (PCz), the electronic band gap E_g defined as the onset for the π^-/π^* interband transition is close to 3.2 eV (118). The HOMO level for a PCz- 3,6/2,7 copolymer (Co1) and PCz-2,7 homopolymer (Ho1) was reported to be −5.33 and −5.47 eV (119). The E_g calculated from the UV−vis absorption onset of the films were both 2.9 eV. The LUMO levels in film were estimated to be −2.43 and −2.57 eV, respectively. For an electrochemically stable macrocyclic poly(*N*-(2-ethylhexyl)-carbazol-3,6-diyl) (MC1), the HOMO and LUMO energy levels are −5.0 and −1.6 eV, respectively (120). For an electropolymerized dendrimer carbazole (DG2), the HOMO is −5.2 and the LUMO is −2.0 (46). Comparison of these values show that the [PCEMMA/CCP]$_n$ (LbL) have a band gap of 2.9 eV which is lower than a highly cross-linked system in the electropolymerized dendrimer, while the [PCEMMA/CCP/TiO$_x$]$_n$ (LbLT) at 3.3. eV is between that of a PVK film and electropolymerized dendrimer. It should be interesting then to utilize the [PCEMMA/CCP]$_n$ in an OLED device configuration given the HOMO that is higher than PVK.

Further explanations of electrochemical interactions between polymeric materials-TiO$_x$ may have also invoked the protonation of the oxide template, according to

$$Ti^{IV}O_2 + H^+ + e^- \rightarrow Ti^{III}O(OH)$$

So far, this behavior has been encountered only in TiO$_2$ templates that were dip-coated in PEDOT-PSS films (104).

From a general point of view, sol−gel derived organic−inorganic hybrid materials have shown promising results as photovoltaic devices, when organic chromophores are covalently linked to Si−O−Ti units (105). The combined use of carbazole-based materials and titanium oxide have been shown to give interesting results (as hybrid junction systems) for the fixation of atmospheric N_2 (106), although confining/dielectric features for TiO$_x$ have been hardly reported so far. There is indeed a further need for comprehension of the factors that trigger the current decrease including levels of porosity and the thickness of these layers. An immediate consequence could be the use of TiO$_x$ xerogel as a "directing" material for polymers bearing electroactive carbazole units: pairing LbL and surface sol−gel process could confine the electropolymerizable units within the given slabs and thus limit the hole-transporting materials in terms of E_g and position in devices.

Spectroscopic Studies. The UV−vis and photoluminescence spectra (Figure 8) of the hybrid, ultrathin film deposited on ITO substrates were recorded before and after electropolymerization. The UV−vis spectra of the film deposited on ITO prior to electropolymerization is best seen in Figure 1. From the UV−vis data, it can be evinced that electrochemical oxidation (i.e., doping) of conjugated polymers decreases the $\pi-\pi^*$ band at 297 nm of the carbazole units (91). Moreover, closer inspection reveals the appearance of a new broad band that stretches from ca. 400 to over 500 nm. This is associated with the formation of the polaronic state of the π-conjugated polycarbazole, proof that the electropolymerization resulted in radical cation coupling of the carbazole (91). Comparison with solution spectra according to literature at λ_{max} = 384 nm (since the electropolymerized films are fixed on the substrate) reveal broadening and red shift of the film absorption spectra, which indicate aggregations or $\pi-\pi$ interactions of the polymer chains in the solid state (118). The photoluminescence spectra of the films are also shown in Figure 8. The large Stokes shift (from 297 nm in Figure 1 to 360 nm) is apparently predetermined by the more polar and electrostatic LbL environment, which better stabilizes the excited state than the ground state, and by the large difference in the structures of the excited and the ground state. Comparison of the photoluminescence spectra (excitation wavelength 300 nm), before and after CV, showed an analogous

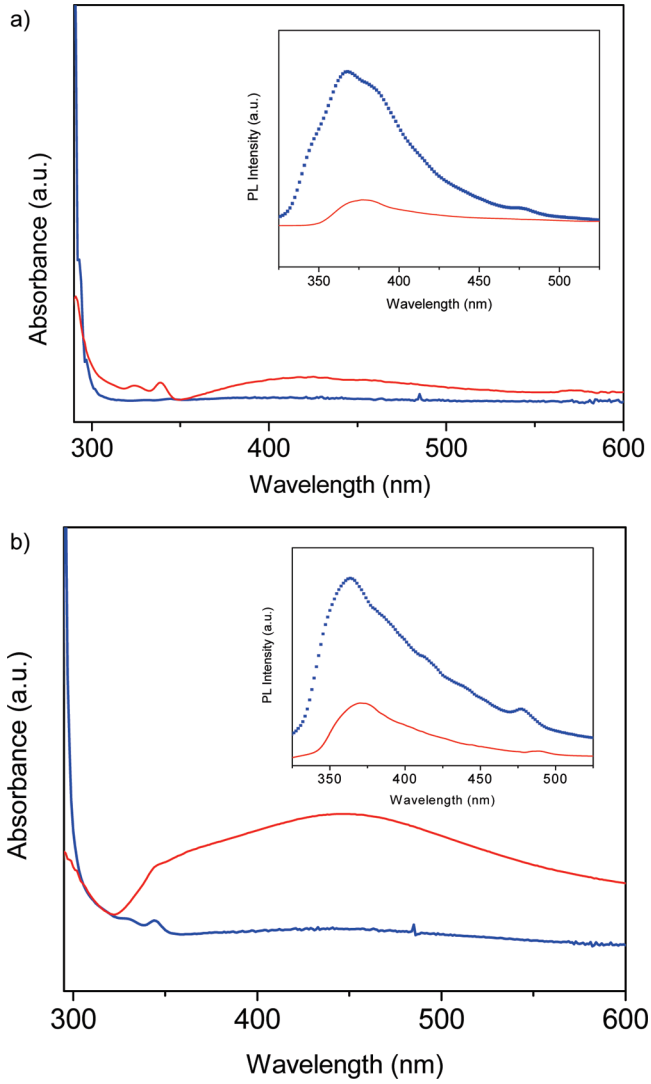

FIGURE 8. Absorption/emission (insets) of (a) PCEMMA/CCP/TiO_x and (b) PCEMMA/CCP films before (blue, squares) and after (red, solid lines) electropolymerization.

trend; a decrease of the emission intensity. This change could be attributed to the immobilization of the polymeric chains subsequent to cross-linking, as well as lesser availability of monomeric carbazole units to absorb the excitation radiation (300 nm) as the cross-linking proceeds. Other phenomena, such as packing and morphology changes, might also be present (85). The overall effect is still a decrease of the emission.

Finally, the optical behavior of the film without inorganic counterparts was evaluated also by UV−vis and fluorescence: comparison of its absorption/emission to those of the hybrid architecture was done before and after electropolymerization (Figure 8). Interestingly, the extension of cross-linking among carbazole units may be quantitatively estimated from the intensity of the polaronic band in the absorption spectrum (91). The quenching in the photoluminescence spectra (excitation wavelength 300 nm in both cases) appears slightly different (Figure 8, insets), in that intercalation with the inorganic slabs produced a more marked decrease on the photoluminescence intensity (350 nm) after cross-linking. This can be readily seen by comparing the post-CV decrease in the hybrid, organic−inorganic film (Figure 8a) to the post-CV decrease in the all organic PCEMMA/CCP film (Figure 8b). In this case, it is also possible that the absorbance property of the, TiO_x layer, a known absorber at the UV spectrum could attenuate the ability to populate more excited states for the carbazole once it is electropolymerized to polycarbazole (108). Note that amorphous TiO_x prepared by sol−gel is not to be confused with high temperature prepared crystalline TiO_x which is photocatalytic (109).

This strongly confirms the general idea of chain immobilization (85) because of the electrochemical cross-linking (i.e., a tighter entanglement of the polymer backbones occurs, the likelihood of nanodomains and aggregates therefore increases), and confining behavior that TiO_x imparts to the film. In the future, it should be of interest to investigate the energy transfer characteristics and fluorescence lifetimes of the polycarbazoles in such confined environments under waveguide structures - to take advantage of the thin film quantitative nanostructuring (110). It is also possible to observe applications of such films toward electrochemical behavior in LbL films (121). We are currently in the process of studying the reciprocal relationships among CV-induced polymerization in polythiophene precursors and spectroscopic behavior in similar, hybrid nanocomposite ultrathin films.

CONCLUSIONS

The LbL self-assembly of intercalated of polycarbazole precursors PCEMMA/CCP polyelectrolyees with slabs of sol−gel-processed TiO_x were investigated and characterized for their deposition, electropolymerization, and electro-optical properties. Linear film growth (in terms of absorbance increment, thickness, frequency shifts) was monitored through UV−vis spectroscopy, optical ellipsometry and QCM-*D* measurements. Upon cyclic voltammetry and subsequent anodic electrochemical oxidation of the carbazole pendant units within the polyelectrolyte layers, a CPN film was quantitatively realized and observed. The current peaks varied as a function of the inorganic slabs, namely it was found that TiO_x showed attenuating/dielectric behavior onto the CV-driven anodic oxidation. Further spectroscopic measurements confirmed the electrochemical conversion and comparison of the band gap energy made with other polycarbazole derivatives. The carbazole units retained their electroactivity upon intercalation of sol−gel-cast TiO_x, demonstrating that the combination of an LbL electrostatic assembly and surface sol−gel process affords layered hybrid nanomaterials that may have practical applications in charge-carrier hole transport in semiconductor devices.

Acknowledgment. The authors acknowledge funding from NSF DMR-10-06776, CBET-0854979, Texas NHARP 01846, and Robert A. Welch Foundation, E-1551. Technical support from Biolin (KSV Instruments), Optrel GmBH, Metro-Ohm Inc. is also acknowledged, and Chengyu Huang for the synthesis of PCEMMA polyelectrolytes.

REFERENCES AND NOTES

(1) Decher, G. *Science* **1997**, *277*, 1232–1237.
(2) Mitzi, D. B. *Funct. Hybrid Mater.* **2004**, 347–386.
(3) Podsiadlo, P.; Shim, B.; Kotov, N. *Coord. Chem. Rev.* **2009**, *253*, 2835–2851.
(4) Ariga, K.; Ji, Q.; Hill, J.; Vinu, A. *Soft Matter* **2009**, *5*, 3562–3571.
(5) Lutkenhaus, J.; Hammond, P. *Soft Matter* **2007**, *3*, 804–816.
(6) Hüsing, N.; Schubert, U. In *Functional Hybrid Materials*; Wiley-VCH Verlag GmbH & Co.: Weinheim, 2004.
(7) Caruso, R.; Antonietti, M. *Chem. Mater.* **2001**, *13*, 3272–3282.
(8) Ichinose, I.; Kunitake, T. *Chem. Lett.* **2001**, *7*, 626–627.
(9) Keller, S. W.; Kim, H.-N.; Mallouk, T. E. *J. Am. Chem. Soc.* **1994**, *116*, 8817–8818.
(10) Judeinstein, P.; Sanchez, C. *J. Mater. Chem.* **1996**, *6*, 511–525.
(11) Nicole, L.; Boissiere, V.; Grosso, D.; Quach, A.; Sanchez, C. *J. Mater. Chem.* **2005**, *15*, 3598–3627.
(12) Cao, G.; Hong, H.-G.; Mallouk, T. E. *Acc. Chem. Res.* **1992**, *25*, 420–427.
(13) Katz, H. E.; Schilling, M. L. *Chem. Mater.* **1993**, *5*, 1162–1166.
(14) Kepley, L. J.; Sackett, D. D.; Bell, C. M.; Mallouk, T. E. *Thin Solid Films* **1992**, *208*, 132–136.
(15) Dodabalapur, A.; Torsi, L.; Katz, H. E. *Science* **1995**, *268*, 270–271.
(16) Baba, A.; Park, M.-K.; Advincula, R. C.; Knoll, W. *Langmuir* **2002**, *18*, 4648–4652.
(17) Park, M.-K.; Onishi, K.; Locklin, J.; Caruso, F.; Advincula, R. C. *Langmuir* **2003**, *19*, 8550–8554.
(18) Blodgett, K. B. *J. Am. Chem. Soc.* **1935**, *57*, 1007–1022.
(19) Ulman, A. In *An Introduction to Ultrathin Organic Films: From Langmuir—Blodgett to Self-Assembly*; Academic Press: Boston, MA, 1991.
(20) Stockton, W.; Rubner, M. *Macromolecules* **1997**, *30*, 2717–2725.
(21) Vázquez, E.; Dewitt, D.; Hammond, P.; Lynn, D. *J. Am. Chem. Soc.* **2002**, *124*, 13992–13993.
(22) Kharlampieva, E.; Kozlovskaya, V.; Sukhishvili, S. *Adv. Mater.* **2009**, *21*, 1–13.
(23) Kim, J.; Tripathy, S. K.; Kumar, J.; Chittibabu, K. G. *Mater. Sci. Eng., C* **1999**, *11*, 2250–2256.
(24) Lee, S.-W.; Ichinose, I.; Kunitake, T. *Chem. Lett.* **2002**, *7*, 678–679.
(25) Advincula, R.; Baba, A.; Kaneko, F. *Colloids Surf. A* **2000**, *173*, 39–49.
(26) Truijen, I.; Bael, M. K.; Rul, H.; D'Haen, J.; Mullens, J. *J. Sol—Gel Sci. Technol.* **2007**, *43*, 291–297.
(27) Advincula, R.; Aust, E.; Meyer, W.; Knoll, W. *Langmuir* **1996**, *12*, 3536.
(28) Ferguson, G. S.; Kleinfeld, E. R. *Science* **1994**, *265*, 370–373.
(29) Park, M.-K.; Onishi, K.; Locklin, J.; Caruso, F.; Advincula, R. C. *Polym. Mater. Sci. Eng.* **2003**, *89*, 312–313.
(30) Advincula, M.; Rahemtulla, F.; Advincula, R.; Ada, E.; Lemons, J.; Bellis, S. *Biomaterials* **2006**, *27*, 2201–2212.
(31) Advincula, M.; Rahemtulla, F.; Advincula, R.; Peterson, D.; Lemons, J. *J. Biomed. Mater. Res. B* **2007**, *80B*, 107–120.
(32) Ichinose, I.; Senzu, H.; Kunitake, T. *Chem. Lett.* **1996**, *10*, 831–832.
(33) F. Huguenin, F.; Ferreira, M.; Zucolotto, V.; Nart, F. C.; Torresi, R. M.; Oliveira, O. N. *Chem. Mater.* **2004**, *16*, 2293–2299.
(34) *Handbook of Conducting Polymers*; Skotheim, T. A., Elsenbaumer, R. L., Reynolds, J. R., Eds.; Marcel Dekker: New York, 1998.
(35) Malinauskas, A.; Malinauskiene, J.; Ramanavicius, A. *Nanotechnology* **2005**, *16*, R51–R62.
(36) Zhang, X.; Xu, Y.; Sun, Y.; Shi, H.; Zhu, X.; Cao, Y. *Thin Solid Films* **2007**, *515*, 7347–7351.
(37) Ravindranath, R.; Ajikumar, P. K.; Bahulayan, S.; Hanafiah, N. B. M.; Baba, A.; Advincula, R. C.; Knoll, W.; Valiyaveettil, S. *J. Phys. Chem. B* **2007**, *111*, 6336–6343.
(38) Zeng, W.; Wu, H.; Zhang, C.; Huang, F.; Peng, J.; Yang, W.; Cao, Y. *Adv. Mater.* **2007**, *19*, 810–814.
(39) Huang, H.; He, Q.; Lin, H.; Bai, F.; Cao, Y. *Thin Solid Films* **2005**, *477*, 7.
(40) Xu, Y.; Peng, J.; Mo, Y.; Hou, Q.; Cao, Y. *Appl. Phys. Lett.* **2005**, *86*, 163502/1.
(41) Zhang, X.; Chen, Z.; Yang, C.; Li, Z.; Zhang, K.; Yao, H.; Qin, J.; Chen, J.; Cao, J. *Chem. Phys. Lett.* **2006**, *422*, 386–390.
(42) Baba, A.; Onishi, K.; Knoll, W.; Advincula, R. *J. Phys. Chem. B.* **2004**, *108*, 18949–18955.
(43) Inaoka, S.; Roitman, D. B.; Advincula, R. *Chem. Mater.* **2005**, *17*, 6781–6789.
(44) Jagadesan, S.; Advincula, R.; Valiyaveettil, S. *Adv. Mater.* **2005**, *17*, 1282–1285.
(45) Xia, C.; Advincula, R. *Chem. Mater.* **2001**, *13*, 1682–1691.
(46) Taranekar, P.; Fulghum, T.; Baba, A.; Patton, D.; Ponnapati, R.; Clyde, G.; Advincula, R. *J. Am. Chem. Soc.* **2007**, *129*, 12537–12548.
(47) Fulghum, T.; Karim, S. M. A.; Baba, A.; Taranekar, P.; Nakai, T.; Masuda, T.; Advincula, R. C. *Macromolecules* **2006**, *39*, 1467–1473.
(48) Waenkaew, P.; Taranekar, P.; Phanichphant, P.; Advincula, R. *Macromol. Rapid Commun.* **2007**, *28*, 1522–1527.
(49) Huang, C.; Jiang, G.; Advincula, R. *Macromolecules* **2008**, *41*, 4661–4671.
(50) Jegadesan, S.; Sindhu, S.; Advincula, R.; Valiyaveettil, S. *Langmuir* **2006**, *22*, 3807–3811.
(51) Park, J.; Ponnapati, R.; Taranekar, P.; Advincula, R. *Langmuir* **2010**, *26*, 6167–6176.
(52) Kaewtong, C.; Jiang, G.; Felipe, J.; Pulpoka, B.; Advincula, R. *ACS Nano* **2008**, *2*, 1533–1542.
(53) Chinowsky, T. M.; Saban, S. B.; Yee, S. S. *Sens. Actuators, B* **1996**, *35*, 37–43.
(54) Badia, A.; Arnold, S.; Scheumann, V.; Zizlsperger, M.; Mack, J.; Jung, G.; Knoll, W. *Sens. Actuators, B* **1999**, *54*, 145–165.
(55) Taranekar, P.; Baba, A.; Fulghum, T. M.; Advincula, R. C. *Macromolecules* **2005**, *38*, 3679–3687.
(56) Taranekar, P.; Fulghum, T. M.; Baba, A.; Patton, D.; Advincula, R. C. *Langmuir* **2007**, *23*, 908–917.
(57) Xia, C.; Fan, X.; Park, M.; Advincula, R. *Langmuir* **2001**, *17*, 7893–7898.
(58) Taranekar, P.; Fan, X.; Advincula, R. *Langmuir* **2002**, *18*, 7943–7952.
(59) Deng, S.; Advincula, R. C. *Chem. Mater.* **2002**, *14*, 2184–2191.
(60) Frau, A.; Pernites, R.; Advincula, R. *Ind. Eng. Chem. Res.* **2010**, *49*, 9789–9797.
(61) Huang, Z. H.; Zeng, X. T.; Kang, E.-T.; Fuh, Y. H.; Lu, L. *Surf. Coat. Technol.* **2005**, *198*, 357–361.
(62) Nakada, H. *J. Photopolym. Sci. Technol.* **2007**, *20*, 35–45.
(63) Marques, A. C.; Almeida, R. M. *J. Sol—Gel Sci. Technol.* **2006**, *40*, 371–378.
(64) Kim, J. Y.; Kim, S. H.; Lee, H.-H.; Lee, K.; Ma, W.; Gong, X.; Heeger, A. J. *Adv. Mater.* **2006**, *18*, 572–576.
(65) Huang, C.; Jiang, G.; Advincula, R. *Macromolecules* **2008**, *41*, 4661–4670.
(66) Knoll, W. *Annu. Rev. Phys. Chem.* **1998**, *49*, 569–638.
(67) Nyulaszi, L.; Veszpremi, T. *J. Mol. Struct.* **1986**, *140*, 253–260.
(68) Waenkaew, P.; Taranekar, P.; Baba, A.; Huang, C.; Patton, D.; Park, J.-Y.; Fulghum, T. M.; Phanichphant, S.; Advincula, R. C. *PMSE Preprints* **2006**, *94*, 511–512.
(69) Yu, H.; Li, X.-J.; Zheng, S.-J.; Xu, W. *Mater. Chem. Phys.* **2006**, *97*, 59–63.
(70) Kaune, G.; Wang, W.; Metwalli, E.; Ruderer, M.; Roβner, R.; Roth, S. V.; Müller-Buschbaum, P. *Eur. Phys. J. E* **2008**, *26*, 73–79.
(71) Sauerbrey, G. *Z. Phys.* **1959**, *155*, 206–222.
(72) Bailey, L.; Kambhampati, D.; Kanazawa, K.; Knoll, W.; Frank, C. *Langmuir* **2002**, *18*, 479–489.
(73) Buttry, D. Applications of the QCM to Electrochemistry. In *A Series of Advances in Electroanalytical Chemistry;* Bard, A., Dekker, M., Eds.; New York, 1991.
(74) Baba, A.; Tian, S.; Stefani, F.; Xia, C.; Wang, Z.; Advincula, R. C.; Johannsmann, D.; Knoll, W. *J. Electroanal. Chem.* **2004**, *562*, 95–103.
(75) Lu, C. S.; Lewis, O. *J. Appl. Phys.* **1972**, *43*, 4385–4390.
(76) Voinova, M. V.; Rodahl, M.; Jonson, M.; Kasemo, B. *Phys. Scr.* **1999**, *59*, 391–396.
(77) White, C. C.; Schrag, J. L. *J. Chem. Phys.* **1999**, *111*, 11192–11206.
(78) Vogt, B. D.; Lin, E. K.; Wu, W.-l.; White, C. C. *J. Phys. Chem.* **2004**, *108*, 12685–12690.
(79) Vogt, B. D.; Soles, C. L.; Lee, H.-J.; Lin, E. K.; Wu, W.-l. *Langmuir* **2004**, *20*, 1453–1458.
(80) Notley, S. M.; Eriksson, M.; Wågberg, L. *J. Colloid Interface Sci.* **2005**, *292*, 29–37.
(81) Norgren, M.; Gärdlund, L.; Notley, S. M.; Htun, M.; Wågberg, L. *Langmuir* **2007**, *23*, 3737–3743.

(82) Roncali, *J. Chem. Rev.* **1992**, *92*, 711–730.
(83) Geissler, U.; Hallensleben, M. L.; Riecken, A.; Rohde, N. *Synth. Met.* **1997**, *84*, 375–380.
(84) Morin, J.-F.; Leclerc, M. *Macromolecules* **2001**, *34*, 4680–4682.
(85) Xia, C.; Advincula, R. C. *Chem. Mater.* **2001**, *13*, 1682–1691.
(86) Morin, J.-F.; Leclerc, M. *Macromolecules* **2002**, *35*, 8413–8417.
(87) Inzelt, G. *J. Sol. St. Electrochem.* **2003**, *7*, 503–509.
(88) Iraqi, A.; Wataru, I. *Chem. Mater.* **2004**, *16*, 442–448.
(89) Thomas, C. A.; Zong, K.; Abboud, K. A.; Steel, P. J.; Reynolds, J. R. *J. Am. Chem. Soc.* **2004**, *126*, 16440–16450.
(90) Iraqi, A.; Pickup, D.; Yi, H. *Chem. Mater.* **2006**, *18*, 1007–1015.
(91) Taranekar, P.; Fulghum, T.; Patton, D.; Ponnapati, R.; Clyde, G.; Advincula, R. *J. Am. Chem. Soc.* **2007**, *129*, 12537–12548.
(92) Ambrose, J.; Carpenter, L.; Nelson, R. *J. Electrochem. Soc.* **1975**, *122*, 876–894.
(93) Romero, D.; Nuesch, F.; Benazzi, T.; Adès, D.; Siove, A.; Zuppiroli, L. *Adv. Mater.* **1997**, *9*, 1158–1164.
(94) Mengoli, G.; Musiani, M. M.; Schreck, B.; Zecchin, S. *J. Electroanal. Chem.* **1988**, *246*, 73–80.
(95) Cattarin, S.; Mengoli, G.; Musiani, M. M.; Schreck, B. *J. Electroanal. Chem.* **1988**, *246*, 87–100.
(96) Siove, A.; Adès, D.; N'gbilo, E.; Chevrot, C. *Synth. Met.* **1990**, *38*, 331–340.
(97) Pelous, Y.; Froyer, G.; Adès, D.; Chevrot, C.; Siove, A. *Polym. Comm.* **1990**, *31*, 341–344.
(98) Marrec, P.; Dano, C.; Gueguen-Simonet, N.; Simonet, J. *Synth. Met.* **1997**, *89*, 171–179.
(99) Crespilho, F.; Zucolotto, V.; Oliveira, Jr., O.; Nart, F. *Int. J. Electrochem. Sci.* **2006**, *1*, 194–214.
(100) Rmaile, H.; Schlenoff, J. *J. Am. Chem. Soc.* **2003**, *125*, 6602–6603.
(101) Abe, K.; Ishii, A.; Hirano, M.; Rusling, J. *Electroanalysis* **2005**, *24*, 2266–2272.
(102) Zotti, G.; Schiavon, G.; Zecchin, S.; Morin, J.-F.; Leclerc, M. *Macromolecules* **2002**, *35*, 2122–2128.
(103) Tan, S.; Su, B.; Roussel, C.; Girault, H. H. *Inorg. Chim. Acta* **2008**, *361*, 746–760.
(104) Cuentas-Gallegos, A. K.; Rincón, M. E.; Orozco-Gamboa, G. *Electrochim. Acta* **2006**, *51*, 3794–3801.
(105) Lin, C.-L.; Yeh, M.-Y.; Chen, C.-H.; Sudhakar, S.; Luo, S.-J.; Hsu, Y.-C.; Huang, C.-Y.; Ho, K.-C.; Luh, T.-Y. *Chem. Mater.* **2006**, *18*, 4157–4162.
(106) Ogawa, T.; Igarashi, T.; Kawanishi, T.; Kitamura, T.; Hoshino, K. *J. Photopolym. Sci. Technol.* **2004**, *17*, 143–150.
(107) Ozcicek, N. P.; Pekmez, K.; Holze, R.; Yildiz, A. *J. Appl. Polym. Sci.* **2003**, *90*, 3417–3423.
(108) Levy, D.; Esquivias, L. *Adv. Mater.* **1995**, *7*, 120–129.
(109) Watanabe, T.; Nakajima, A.; Wang, R.; Minabe, M.; Koizumi, S.; Fujishima, A.; Hashimoto, K. *Thin Solid Films* **1999**, *351*, 260–263.
(110) Bahat, A.; Bouazaoui, M.; Bahtat, M.; Garapon, C.; Jacquier, B.; Mugnier, J. *J. Non-Cryst. Solids* **1996**, *202*, 16–22.
(111) Cloutet, E.; Yammine, P.; Ades, D.; Siove, A. *Synth. Met.* **1999**, *102*, 1302–1303.
(112) Tsakova, V.; Winkels, S.; Schultze, J. *Electrochim. Acta* **2000**, *46*, 759–776.
(113) Schlenoff, J.; Ly, H.; Li, M. *J. Am. Chem. Soc.* **1998**, *120*, 7626–7634.
(114) Berlin, A. In *Electrical and Optical Polymer System—Fundamentals, Methods, and Applications*; Wise, D. L., Wnek, G. E., Trantolo, D. J., Cooper, T. M., Gresser, J. D., Eds.; Marcel Dekker: New York, 1993;p 47.
(115) Sze, S. M. In *Physics of Semiconductor Devices*, 2nd ed.; Wiley: New York, 1981; p 245.
(116) Zhanh, Z.; Jiang, X.; Xu, S.; Nagatomo, T.; Omoto, O. *Synth. Met.* **1997**, *91*, 131–132.
(117) Parker, I. *J. Appl. Phys.* **1994**, *75*, 1656–1666.
(118) Tran-Van, F.; Henri, T.; Chevrot, C. *Electrochim. Acta* **2002**, *47*, 2927–2936.
(119) Yang, L.; Feng, J.; Ren, A.; Sun, J. *Polymer* **2006**, *47*, 1397–1404.
(120) Ostrauskaite, J.; Strohriegl, P. *Macromol. Chem. Phys.* **2003**, *204*, 1713–1718.
(121) DeLongchamp, D. M.; Hammond, P. T. *Langmuir* **2004**, *20*, 5403–5411.

AM100867Q